^{7}Li Solid-State Nuclear Magnetic Resonance as a Probe of Lithium Species in Microporous Carbon Anodes

Sophia E. Hayes,*,†,‡ Ronald A. Guidotti,§ William R. Even, Jr.,|| Paula J. Hughes,⊥ and Hellmut Eckert†,#

Department of Chemistry, University of California Santa Barbara, Santa Barbara, California 93106, Sandia National Laboratories, Livermore, California 94550, Sandia National Laboratories, Albuquerque, New Mexico 87185, and Eveready Battery Company, Westlake, Ohio 44145

Received: July 31, 2002; In Final Form: February 5, 2003

Electrochemical insertion of lithium into pyrolyzed amorphous carbons prepared from polymeric precursors of methacrylonitrile and divinylbenzene has been investigated by ^{7}Li variable temperature static and magic angle spinning (MAS) NMR. This method is able to characterize the chemical inventory of lithium, differentiating between reversible species that are truly inserted into the carbon and irreversible species that are lost to traps and parasitic processes. Furthermore, large chemical shift effects indicate that the structural and electronic properties of the inserted reversible lithium species are sensitively dependent on the extent of loading. At loading levels ≤90% relative capacity, the trend is monotonic, whereas in more highly charged samples, two types of electrochemically relevant sites are observed, distinguishable from one another only at lower temperatures. At higher temperatures, dynamic exchange effects between them are evident on the NMR time scale. In the initially prepared state, these highly charged materials contain regular intercalated lithium sites as well as clusters of atomic lithium species dispersed in the amorphous matrix. The cluster sites are depopulated with time, a process that can be accelerated by heating.

Introduction

The fundamental study of lithium-intercalated carbons, of both graphitic and amorphous types, is of great interest because of the important role these materials play in the battery and electrochemical energy-storage arenas. In particular, lithiated carbons show promise as anode materials in lithium-ion batteries, as a substitute for metallic lithium, or a lithium alloy.[1−3] Lithium-metal anodes present several problems when used in a rechargeable battery, namely, safety issues related to their reactivity when exposed to air or water and their lifetimes through many charge−discharge cycles. Lithium-intercalated amorphous carbons are useful for anode applications because they avoid the interfacial problems arising from the reversible redeposition of lithium metal when the cell is charged and discharged (e.g., formation of lithium dendrites). Not only are these lithium-intercalated carbons more stable than the metal itself, but it has been reported that amorphous LiC_n systems can tolerate more than 1000 deep charge−discharge cycles.[4]

A number of recent studies have addressed the issues of carbon structure and morphology and their effects on the cyclability and capacity of batteries made with carbon electrodes. The type of carbon being used as an electrode and its precursor material(s) can have a large effect on the resulting electrochemical performance.[5] Graphite intercalation compounds, first-stage LiC_6 and second-stage LiC_{12}, in particular, have been studied extensively. The structure and stoichiometric formula,[6] electronic properties such as the density of states and magnetic susceptibility,[7,8] physical properties such as transport and magnetism,[9−11] the chemical potential of intercalated lithium,[12] and even catalytic properties[13] have all been investigated for this class of materials.

The type of carbon selected for use as an electrode material is usually based on electrochemical performance factors such as high specific reversible capacities, minimal irreversible first-cycle lithium losses, and an ability to cycle repeatedly between charged and discharged states without significant loss of capacity (low fade). The specific capacity for lithiated graphite (LiC_6) is 372 mAh/g, and a number of disordered carbons with specific capacities greater than this have been reported,[14] up to 850 mAh/g[15] in the case of a lithium-doped polyacenic semiconductor. The disordered carbons can be classified into two types: graphitizable ("soft") and nongraphitizable ("hard") carbons. Disordered carbons that are prepared at pyrolysis temperatures below 1000°C are termed "turbostratic"[16] and exhibit random stacking. These have small graphene sheets (20−50 Å in length), stacked in a roughly parallel fashion but with random rotations and translations between pairs of layers. Above 1000°C is the regime where heat treatment of "hard" carbons does not have a demonstrable effect on increasing correlation lengths and inducing an ordering of the material; they never become fully graphitized. In contrast, "soft" carbons can be almost completely graphitized when heated to 3000 °C.

The disordered nature of many of these carbon electrodes may lead to better cell performance compared to graphite. Because of their larger interlayer spacing (compared to graphite) they offer the prospect of longer lifetimes (more cycles) because the distortion of the lattice upon charging and discharging can

* To whom correspondence should be addressed.
† University of California Santa Barbara.
‡ Present address: Department of Chemistry, Washington University, St. Louis, MO 63130.
§ Sandia National Laboratories, Albuquerque.
|| Sandia National Laboratories, Livermore.
⊥ Eveready Battery Company, Westlake, OH 44145.
Present address: Institut für Physikalische Chemie WWU Münster, Germany 48149.

10.1021/jp021772f CCC: $25.00
Published on Web 04/15/2003

be minimized. Recently, disordered and turbostratic carbon materials have become a focus of interest because they appear to allow for significantly higher levels of Li insertion than LiC_6; claims ranging up to the composition LiC_2 have been reported.[17−21] It is worthwhile to note that other applications for these materials have also been considered, such as supercapacitors, catalyst supports, and materials for gas separations,[22] because of the open framework of the carbon and its parent foam.

Variables such as the heat-treatment temperature, whether the carbon is graphitizable (soft) or nongraphitizable (hard), and the hydrogen content of the carbon[23] all have lasting effects on the end products. To this end, carbons of various types have been investigated for use as anode materials. Examples include composite carbons for use in a polymer electrolyte battery,[24] pitch cokes,[25] mesocarbon microbeads,[26−28] polyacrylonitrile-based carbon fibers, and resin-coated graphite powders.[29] These materials have been investigated to explore the effects of structure and morphology on parameters such as the discharge capacities and Coulombic efficiencies, the effect of the crystal structure and surface modification on reactivity with electrolyte solvents,[30] stable capacity with cycling, and the role of heteroatoms (e.g., nitrogen, oxygen, and hydrogen) on irreversible lithium losses.[25] Many of these studies have found that carbon materials with disordered structures have higher capacities than graphitic carbon materials.

The source of carbon for the electrodes under investigation here is a disordered foam, synthesized from two polymeric precursors (methacrylonitrile and divinylbenzene), through inverse micelle-emulsion techniques. These copolymers form a cross-linked network that stabilizes the foam morphology imparted by the emulsion. This foam is a precursor to the final carbon material that is prepared in a multistep process, described in detail elsewhere.[31] Electrochemical intercalation of lithium into these carbons has never been reported before and is the subject of this study.

The various possible lithium environments that might be produced during electrochemical intercalation of a porous carbon electrode include insertion into small, locally ordered stacks of graphite-like layers (analogous to formation of the graphite intercalation compounds, LiC_6) or in turbostratic regions of disordered stacks. Within these disordered regions, the first coordination sphere of the lithium atoms might contain, besides carbon atoms, residual nitrogen or hydrogen atoms introduced from the precursor and oxygen atoms introduced by the stabilization process, as evidenced by elemental analysis (see the Experimental Section). Alternatively, the intercalation process has been proposed to involve the formation of lithium dimers[32] or small clusters within mesopores or microstructural voids (nanopores). All these environments are sites for electrochemically reactive lithium species. In addition to these reversibly occupied sites, there may be irreversibly formed ionic lithium compounds such as LiOH, Li_2CO_3, or Li-polycarbonate and polyalkoxycarbonate complexes produced at the surface that arise from parasitic passivation processes (i.e., electrochemical decomposition of the organic solvent and supporting electrolyte), or even surface adsorbed lithium transport salts from the electrolyte solution. To develop a better understanding of the relationship between structural properties and electrochemical performance, it is important to differentiate between various types of lithium species present. There are those that are truly reversibly intercalated and those lost to traps. The latter lithium species are either located in the passivation layer or irreversibly bound at chemically reactive sites, such as oxygen and nitrogen.

Being an element-selective, inherently quantitative method sensitive to local environments, solid-state nuclear magnetic resonance (NMR) represents an ideal structural tool for addressing these types of questions.[33] The utility of NMR in studying intercalation compounds is evident, determining the arrangement and dynamics of intercalants, the structure of the host materials, and interactions between the two. Li NMR studies have been conducted on intercalated SnS_2[34] as well as titanium- and vanadium-chalcogenides.[35] The bonding character of the lithium intercalants, their mobility, and the interaction with conduction electrons all can be studied using NMR techniques.

Past applications have already demonstrated the utility of ^{7}Li NMR for probing the local environment and the dynamic characteristics of lithium species in various types of intercalated carbons. The ^{7}Li resonance frequency is very sensitive to the conduction electron density located at the lithium site (i.e., the Knight shift) and thus provides useful information about the extent of guest−host charge transfer in these materials. This has been demonstrated amply in the NMR studies of crystalline lithium-graphite intercalation compounds,[36] lithiated disordered hard carbons prepared from organic pitch,[37−39] natural graphite,[40,41] and heat-treated mesocarbon microbeads,[28] as well as numerous types of lithiated soft carbons.[26,28] The review of the literature on this subject reveals a great diversity of spectroscopic characteristics, and resonance shifts ranging from near zero to above one hundred ppm vs aqueous LiCl solution have been reported.[42,43] In many systems, the ^{7}Li resonance shifts measured correlate with the pyrolysis temperature of the carbon used. For example, the chemical shifts of Li-inserted carbon microbeads range from 7 to 45 ppm over the pyrolysis temperature range of 700−3000 °C.[28] Furthermore, the charging state has an important influence, and hysteresis effects upon charging (reduction) and discharging (oxidation) are commonplace. In addition, large chemical shift ranges and unexpected changes of chemical shift with temperature have been observed in these systems.[44,45] Furthermore, many amorphous intercalated carbons tend to display multiple lithium environments, which have been identified and tentatively assigned to distinct bonding states in various amorphous carbon intercalates.[23,37] Hard carbons produce temperature-dependent high frequency resonances upon full intercalation, whereas soft carbons exhibit only low-frequency resonances upon full intercalation without large differences in chemical shift.[46]

In this contribution, we report on the disposition and distribution of various lithium species that result from the insertion of Li into disordered (hard) carbons derived from poly(methacrylonitrile) (PMAN)-divinylbenzene (DVB) precursors pyrolyzed at temperatures of 1100 °C. Through a study of the NMR spectra at various stages of the intercalation process, we attempt to develop a more complete understanding of the structural and dynamic aspects and issues associated with the Li intercalation process into these interesting materials.

Experimental Section

Starting materials were emulsion-derived foams of PMAN and divinylbenzene (DVB) precursors. The molar ratio of methacrylonitrile to DVB was 1.7:1. The copolymer was oxidatively stabilized at 240°C for 12 h prior to pyrolysis at temperatures of 1100 °C for 5 h in a 95% Ar/5% H_2 atmosphere to yield microporous carbons, as reported in detail elsewhere.[31] Chemical analysis reveals typical elemental compositions of 95.46% C, 4.75% N, 1.44% O, and <0.5% H.

Lithium intercalation was carried out at Eveready Battery Company and at Sandia National Laboratories, Albuquerque,

NM. Some of the carbons were prepared for electrochemical testing in an argon glovebox, where the oxygen and moisture levels were maintained at <1 ppm each. Other samples were prepared in a dry room maintained at <3% relative humidity. The electrolyte was 1 M $LiPF_6$ in a mixed ethylene carbonate (EC)/dimethyl carbonate (DMC) solvent (1:1 volume ratio). The test cell was a Swagelok "Tee" and consisted of a working electrode made from a carbon-foam pellet without binder and counter and reference electrodes of lithium metal foil (Foote Mineral). The water content of the solution as measured by Karl Fischer titration was typically <40 ppm.

The anode was separated from the 0.25-mm-thick counter electrode by two Celgard 2500 polypropylene separators. The mass of active carbon ranged from 2 to 6 mg. Cell assembly was conducted in a dry room maintained at a dew point of less than −60°C. The cells were evacuated and backfilled with the electrolyte solution in an argon-filled glovebox where the moisture and oxygen content were <1 ppm each. This procedure ensures good wetting of the separator by the electrolyte.

Typical parameters for the electrochemical performance of PMAN/DVB carbons during galvanostatic cycling are listed below (Table 1). Q_{tot} is the total capacity after the cycle indicated. Q_{rev} is the amount of reversible capacity for that cycle, and Q_{irr} is the amount of irreversible capacity that is lost due to traps or parasitic processes, such as development of the solid-electrolyte interface (SEI) layer.

Galvanostatic testing of the cells was performed using an Arbin Corp. Battery Test System. The test profile consisted of galvanostatic cycling by constant current lithiation and de-lithiation at 0.5 mA/cm^2 (nominal C/5 rate) and 25°C. The cycling potential ranged from 3.0 to 0.0 V versus Li/Li$^+$ for Eveready's samples and 2.0 to 0.01 V versus Li/Li$^+$ for Sandia's samples. Samples for NMR study were cycled between fully intercalated and deintercalated stages in excess of 10 cycles, typically 20, to ensure steady-state processes. At that point, no additional lithium losses to parasitic processes were observed, and the reversible cycle-to-cycle efficiency was greater than 99%. After galvanostatic cycling, the samples were charged up to the desired loading level on the basis of the determined Q_{rev} value. An open-circuit wait of 600 s was imposed between charge and discharge processes. Cyclic voltammograms (Figure 1) were generated using a Princeton Applied Research model 263 potentiostat. The cell was scanned between voltage limits of 3 and 0.01 V at a sweep rate of 1 mV/s. In most cases, total insertion capacities greater than 450 mAh/g were observed.

The term "relative capacity" is used to denote that fraction of charge applied to a carbon sample relative to its Q_{rev} value for a given cycle. For example, the 1100 °C carbon with a Q_{rev} of 200 mAh/g, charged to approximately 100 mAh/g, would have a relative capacity of 50%. An electrode with a 200% relative capacity is a sample that has been "overcharged" or where an overpotential has been applied, such that metallic lithium begins to plate out onto the electrode surface or in the pores of the carbon. To study the effect of charging state (and possible hysteresis effects), samples were prepared with 33%, 50%, 66%, 90%, 100%, 150%, and 200% relative capacity. Within this series, two samples were prepared by charging (insertion of Li) up to full capacity, followed by discharge (removal of Li) to reach the final loading level. These samples were 90% relative capacity electrodes (charged to 100% followed by a 10% de-lithiation) and 50% relative capacity electrodes (charged to 100% followed by a 50% de-lithiation). The purpose of these latter experiments was to determine whether the sites populated on charging are the same sites that stay populated on discharging, as previously examined by Mori et al.[37] (Note, however, that the work by Mori presented data only for the first cycle, whereas our experiments were conducted on samples cycled in excess of 10 times.)

TABLE 1: Representative Electrochemical Performance of PMAN/DVB Pyrolyzed Carbon

sample	Q_{tot} (mAh/g)	Q_{rev} (mAh/g)	Coulombic efficiency (%)	Q_{irr} (mAh/g)
first cycle	399.1	221.0	54.0	178.1
20th cycle	205.5	200.7	97.3	4.8

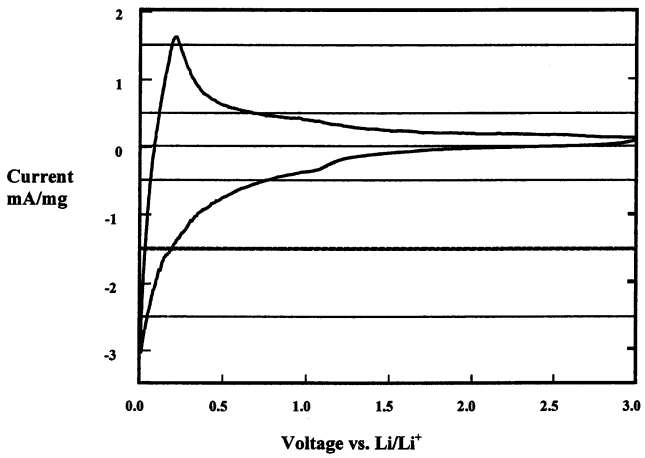

Figure 1. Second-cycle CV for 1100 °C PMAN/DVB.

Solid State NMR Experiments. Samples for NMR analyses were all packed in a glovebox under an argon atmosphere to minimize the amount of exposure of the lithium-intercalated carbons to air and water. Both intercalated and deintercalated samples were examined over a temperature range of 140−400 K by ^{7}Li static and magic-angle spinning (MAS) NMR. All experiments were conducted at 116.8 MHz using a Bruker CXP-300 spectrometer equipped with a Tecmag pulse programmer and acquisition system and a 4 mm high-speed MAS probe. Data acquisition used 90° pulses of approximately 5−7 μs length and 3−4 kHz spinning rates. Additional room-temperature spectra were obtained at 194.49 MHz using Bruker Advance DSX-500 and AMX-500 spectrometers. These experiments utilized 90° pulses of 4 μs length and spinning rates of 6−12 kHz. Relaxation delays used ranged from 1 to 120 s. For variable temperature experiments, typical delays of 1−2 s were used. The ^{7}Li chemical shifts are reported relative to a 1.0 M aqueous solution of LiCl.

Variable temperature experiments were performed on the CXP-300 spectrometer using the 4 mm MAS probe cooled with nitrogen gas flowing through a liquid-nitrogen dewar into the bearing air inlet of the probe. The 4-mm rotors used airtight boron nitride turbine caps that are designed for one-time use. Spinning speeds and temperature were regulated by standard commercial equipment. In most cases, spectra were obtained under both static and MAS conditions using similar acquisition parameters.

Results

Lithium Inventory. Unlike LiC_6, which has a single, unique lithium site centered at approximately 44 ppm, the lithium-intercalated microporous carbons of the present study contain several distinct types of lithium species depending on charging state. As discussed below for several representative samples, four distinct types of sites (A−D**)** can be distinguished, enabling a comprehensive discussion of the lithium inventory throughout the range of materials investigated.

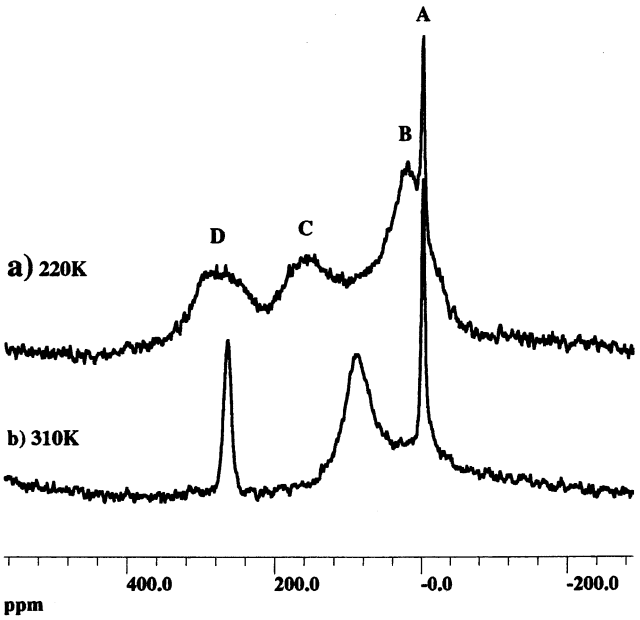

Figure 2. ^{7}Li NMR site assignments of 200% charged carbon electrode at two representative temperatures (220 and 310 K): A = ionic lithium (Li^{+1}), B = low-frequency inserted lithium site, C = high-frequency inserted lithium site, D = lithium metal (Li^0).

Carbon Charged to 200% Relative Capacity. A spectrum showing all observable features for these samples is shown in Figure 2, obtained on a carbon charged to 200% relative capacity at two representative temperatures. This spectrum depicts the coexistence of different bonding states of lithium in the material. Peak A denotes an ionic lithium site, resonating in the vicinity of −1 ppm. Peak B, resonating in the vicinity of 10−15 ppm, denotes an inserted lithium site appearing at a significantly lower resonance shift than that of LiC_6. Note that the intensity of peak B appears diminished at 310 K. Peak C, near 150 ppm (at 200 K), denotes a high frequency inserted lithium site appearing at a substantially larger resonance shift than LiC_6. This value indicates the presence of a large Knight shift, suggesting that the s-electron charge density localized on the lithium ions is substantially increased, lending some metal-like character to these lithium species. Finally, Peak D denotes the metallic lithium site at 264 ppm. The MAS spectra are difficult to simulate because of the large spinning sideband pattern associated with the peak at −1 ppm; therefore, static spectra are typically shown. As Figure 2 indicates, both line widths and resonance shifts are highly temperature-dependent, suggesting the presence of dynamic effects to be discussed in more detail below.

Carbon Charged to 100% Relative Capacity. The electrode charged to 100% of relative capacity has a prominent, broad feature at 100 ppm corresponding to C, and a second sharp feature at −1 ppm arising from A (see Figure 3). From line shape simulations, feature B can also be identified. The static spectrum does not resolve the shift difference between peaks A and B (see Figure 3) because of broadening due to anisotropic interactions; however, the MAS spectrum depicts all three features, with peak B evident as a shoulder next to peak A. This feature is more clearly seen in the variable temperature spectra discussed below. As expected, no elemental lithium is observed in the spectrum of this sample.

Carbon Charged to <100% Relative Capacity. The MAS spectra of these samples reveal the presence of features A and B only (see Figure 4a,b). The chemical shift of peak B depends on the charging state; Figure 4c reveals an approximately linear

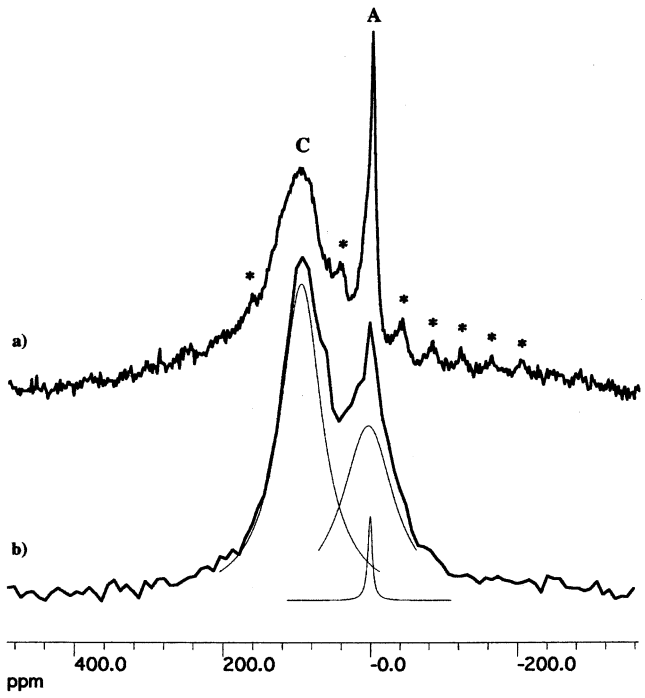

Figure 3. ^{7}Li NMR spectra (room temperature) for 100% charged carbon electrode: (a) MAS spectrum (ν_r = 2.5 kHz) and (b) static spectrum with line simulations as shown. The asterisks indicate spinning sidebands.

relationship with the relative capacity. Only small hysteresis effects are observed. At higher relative capacities, near 90%, the chemical shift increases markedly to approximately 22 ppm (Figure 4c). It is worth noting that both charging to 90% of capacity and charging to 100% followed by discharging by 10% result in similar chemical shifts, differing by only 3−4 ppm. Similarly, electrodes charged to 50% and those charged fully and subsequently discharged by 50% also have nearly identical chemical shifts, differing by only 2 ppm. Our work may be compared to the study of Tatsumi et al. (ref 38) where chemical shift versus charge was examined in lithiated hard carbon fibers upon oxidation and reduction. In that study, a monotonic profile of chemical shift vs relative charge was also observed until within 10% of the maximum reversible capacity.

Interpretation of the observed effect in terms of a Knight shift suggests that the conduction electron density at the lithium atoms increases with increasing lithium content; however, this density remains substantially lower than in LiC_6 (capacity 372 mAh/g, Knight shift 44 ppm). This monotonic dependence of ^{7}Li chemical shifts as a function of charging state contrasts with the staging behavior observed in graphite, where intercalation to a level less than 372 mAh/g results in two-phase materials including higher stage intercalation compounds such as LiC_{12} and LiC_{18}, giving rise to smaller resonance shifts.

Carbon Charged and Subsequently Fully Discharged ("Deintercalated"). Figure 5 shows a typical spectrum of a discharged electrode. Deconvolution reveals that the line shape consists of a sharp feature (A), and a second broad, less intense feature (A′), indicating that a fully discharged electrode has two types of lithium sites. Both central MAS resonances are accompanied by sets of spinning sideband patterns, arising from first-order quadrupolar interactions. This deintercalated carbon sample contains only lithium that has been irreversibly lost to parasitic processes, such as SEI formation, and it lacks ^{7}Li peaks affected by Knight shifts. The broad line (A′) clearly arises as a result of an electrochemical reaction, because it is absent in

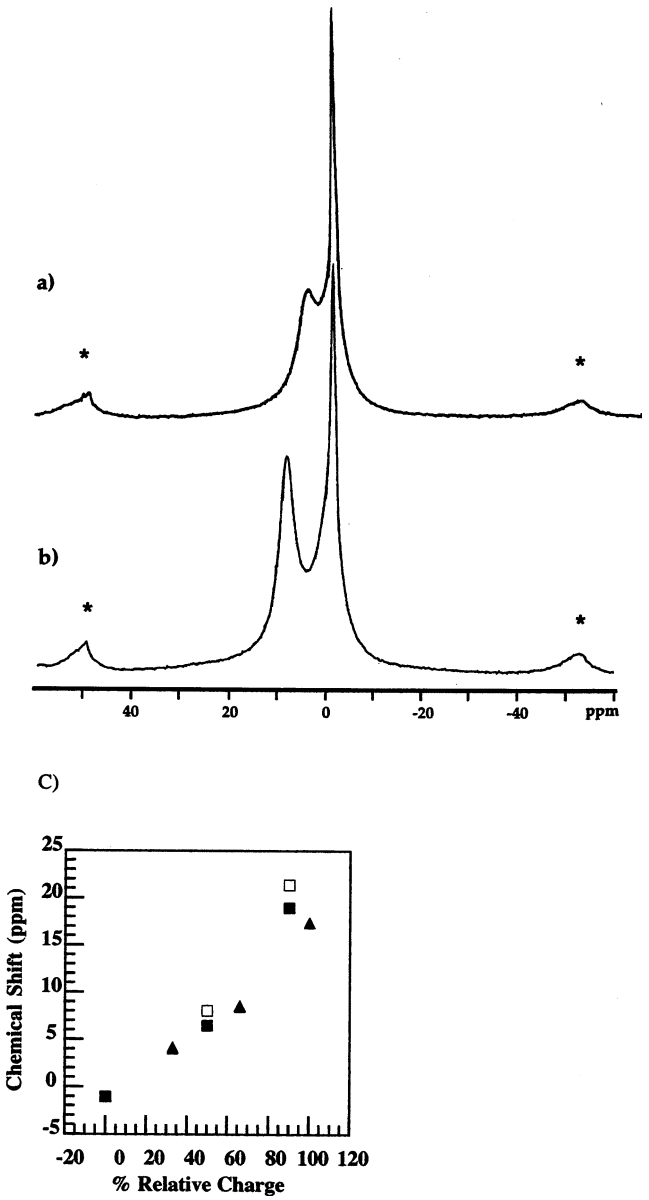

Figure 4. ^{7}Li MAS NMR spectra (room temperature) for carbon electrodes charged to <100% relative capacity: (a) 33%, (b) 66%. The asterisks indicate spinning sidebands. Part c shows correlation of ^{7}Li chemical shift with electrode charging state. Different symbols indicate different batches. Open squares denote discharged samples.

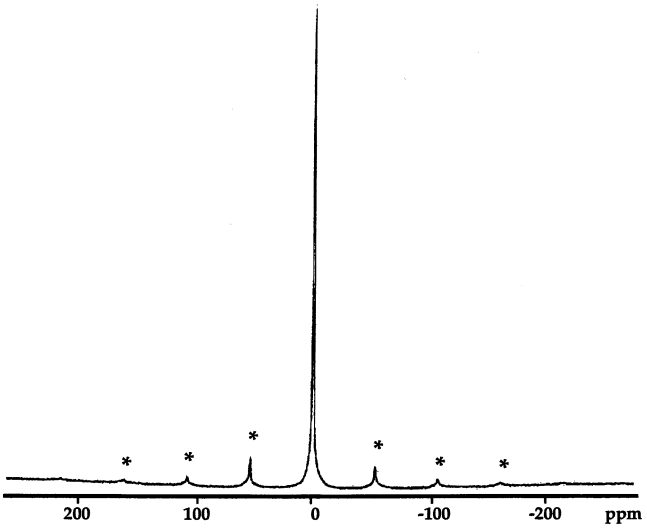

Figure 5. ^{7}Li MAS NMR spectrum for deintercalated carbon electrode (room temperature).

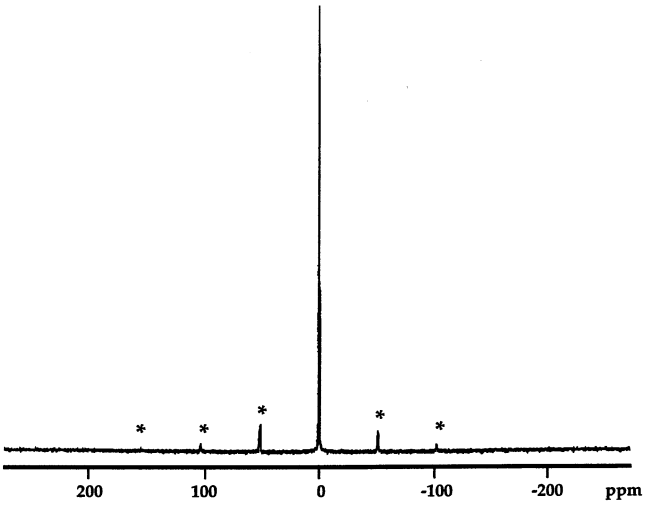

Figure 6. ^{7}Li MAS NMR spectrum for carbon electrode dipped in electrolyte (room temperature).

the spectrum of the carbon electrodes that were not electrochemically cycled. In the spectra of most of the intercalated samples, site A′ is masked by peak overlap and, hence, not included in the spectral deconvolution.

Carbon Electrode Dipped in Electrolyte. The spectrum of this sample is shown in Figure 6. A close inspection of site A at −1 ppm shows that this sample lacks the broad feature (A′) observed in the deintercalated electrode. Because the electrode was merely dipped in the electrolyte and subsequently drained and dried (no electrochemical cycling), the spectrum arises from surface-adsorbed $LiPF_6$/ethylene carbonate/dimethyl carbonate electrolyte. It is also possible that the ionic lithium arises from partially solvated lithium polycarbonate complexes or LiOH wetting the surface. No bulk $LiPF_6$ (NMR signal at −3.15 ppm) was observed in the spectrum.

Carbon Charged and then Subsequently Relaxed. Fully charged samples that have either aged over a period of several months or been heat-treated to 350 K or above display irreversible chemical shift changes in their ^{7}Li spectra. Site C (and D in overcharged samples) is depleted, and typical ^{7}Li shifts of 12−17 ppm are observed, along with substantial peak narrowing (see Figure 7a,b). Similar spectra are observed after heating samples to temperatures of 350−400 K (Figure 7c). Obviously, aging and thermal treatment change the lithium bonding state from one with highly metallic character to one with bonding properties comparable to those of site B in Li intercalation compounds at charging levels ≤100%.

To investigate these time-dependent phenomena in more detail, samples of deintercalated and 200% charged samples were ground and subsequently mixed together and loaded into a rotor for analysis. Figure 7d shows a stackplot of the spectra monitored at different times after mixing. At time zero (15 min after mixing), the coexistence of sites A, C, and D present in the original components is obvious. The most notable time-dependent change is the emergence of a resonance at 14−20 ppm that is attributable to site B. In addition, the chemical shift of site C moves gradually to lower frequencies, although this change is more difficult to detect. The observed time evolution reflects diffusion processes from lithium in the overcharged samples to the deintercalated sample through the SEI layer, whereby unoccupied sites are being populated.

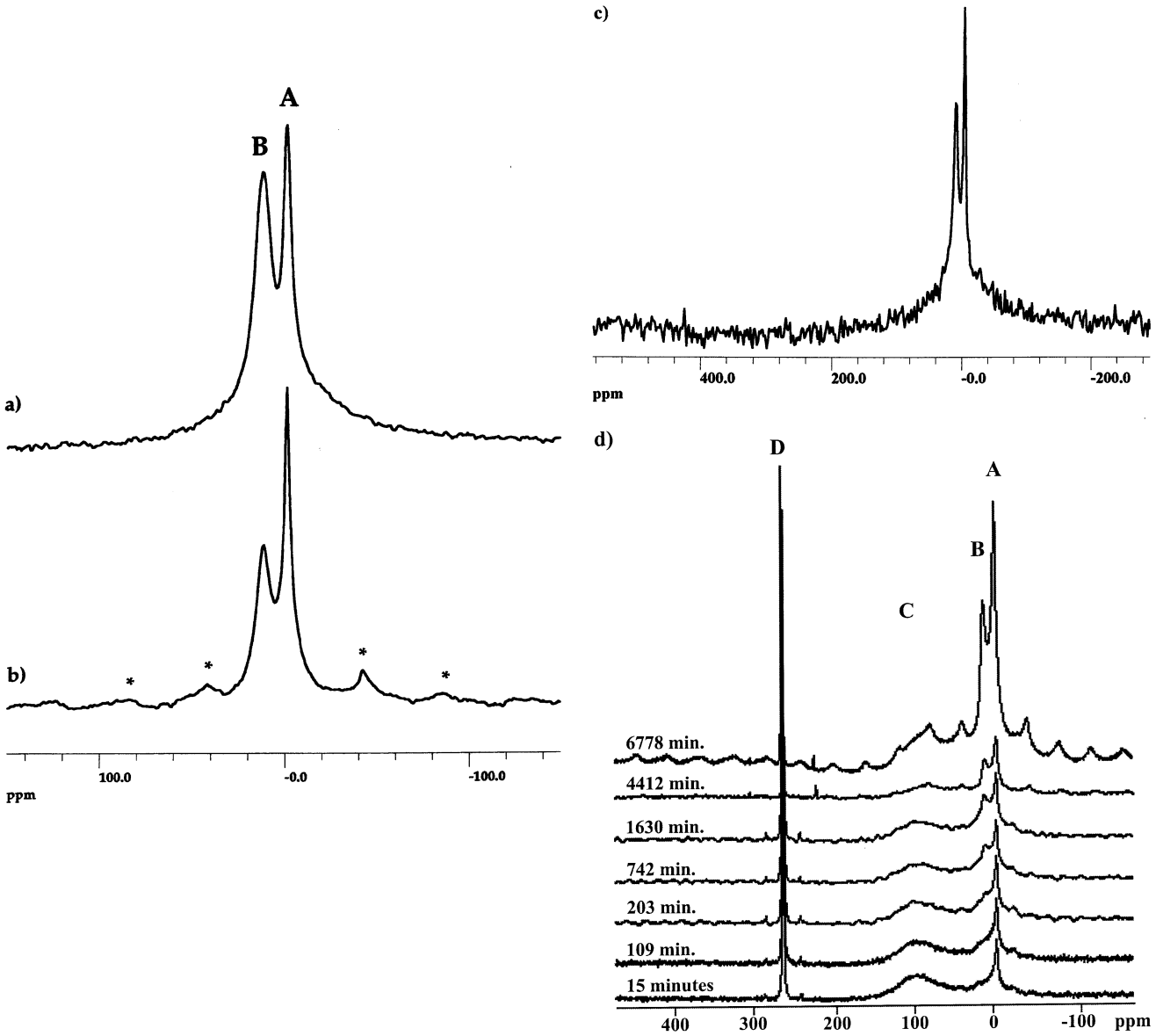

Figure 7. Manifestations of time-dependent chemical relaxation phenomena in lithium−carbon intercalates. Parts a and b show NMR spectra (room temperature) for 100% charged carbon electrodes with a "relaxed" lithium species (a) static spectrum, (b) MAS spectrum ($\nu_r = 4.9$ kHz). Part c shows the spectrum of a 200% charged sample after the sample was heated to 400 K. Part d is a series of time-dependent spectra for a mixture of two electrodes: a 200% charged electrode and a deintercalated electrode. The two were intimately mixed and their NMR spectra monitored over a period of time (as indicated on the figure).

Similar phenomena were observed in samples with nearly no elemental lithium but with a significant site C population. By adding electrolyte, the process can be further accelerated, such that all of the lithium with site C character disappears rapidly, and site B becomes a dominant spectral feature. It is notable that a corresponding control experiment conducted with a carbon electrode that had not been cycled, without the SEI layer, did not reveal any changes on the time scale of this experiment.

Variable Temperature NMR. Based on the above experiments, it is clear that both species B and C reflect electrochemically relevant lithium sites that are reversibly cycled between the charged and the discharged states. Numerous other works have observed similar spectra, and a number of different structural assignments have been proposed. To characterize these sites in more detail and to explore the potential occurrence of dynamic effects, variable temperature (VT) static and MAS NMR experiments were conducted on representative samples. Recycle delays were chosen to ensure relaxation of the electrochemically relevant species, permitting semiquantitative comparisons within experimental error.

The static spectra, summarized in Figure 8, of a 200% charged carbon sample reveal different temperature dependences for the different lithium sites present. The resonance shift of site D is temperature invariant, as expected (and known) for bulk metallic lithium. The shifts of sites A and B are also nearly constant with temperature, whereas site C displays dramatic temperature-dependent effects. At the lowest temperature studied, site C appears strongly shifted to higher frequencies and partially overlaps the resonance, D, of metallic lithium. Furthermore, the line shape of site B becomes increasingly well resolved as the temperature is decreased.

As the temperature is increased, peak C gradually shifts to lower frequencies, whereas peak B decreases in relative intensity. Figure 9 summarizes the temperature dependence of (a) the chemical shifts measured for species B−D, (b) the line

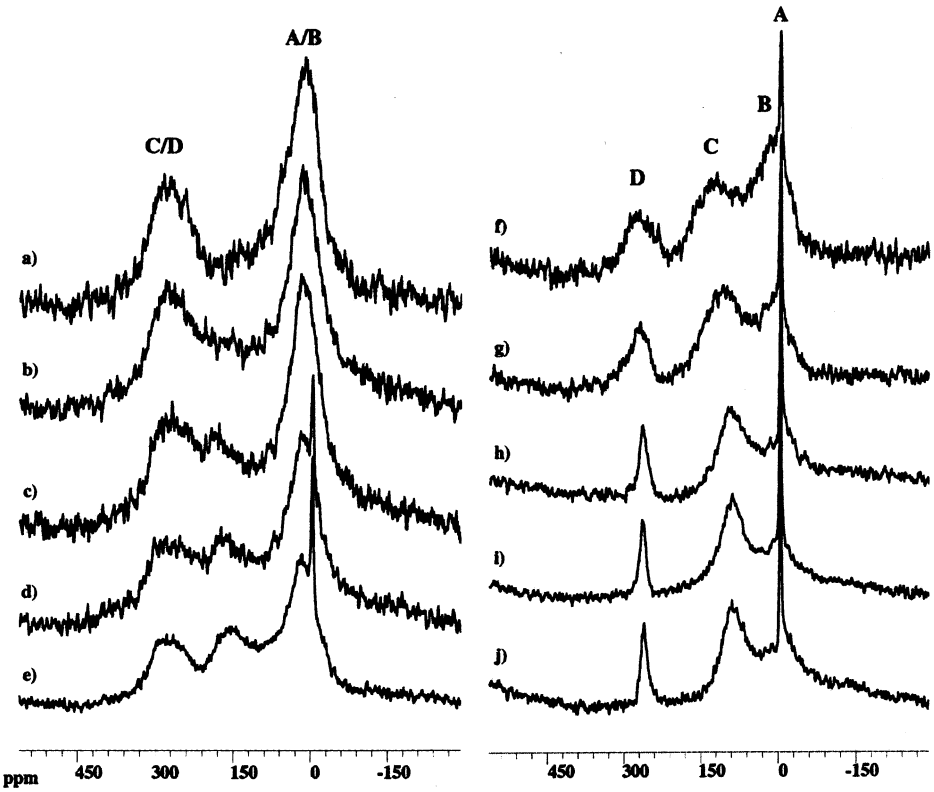

Figure 8. Variable temperature ^{7}Li static NMR spectra of a 200% charged carbon (a) 140, (b) 160, (c) 180, (d) 200, (e) 220, (f) 240, (g) 260, (h) 280, (I) 300, and (j) 310 K.

TABLE 2: Lithium NMR Shifts and Site Assignments in Typical Carbon Samples Studied

sample	^{7}Li chemical shift (ppm)	description
amorphous fully charged carbon, 150%−200% relative capacity	−1 to 0	(A) ionic Li^{+1}
	10 to 15	(B) low-frequency inserted Li^{0-1}
	21 to 120	(C) high-frequency inserted Li^{0-1}
	264	(D) metallic Li^0 (when overcharged)
amorphous fully charged carbon, 100% relative capacity	−1 to 0	(A) ionic Li^{+1}
	10 to 15	(B) low-frequency inserted Li^{0-1}
	21 to 120	(C) high-frequency inserted Li^{0-1}
amorphous partially charged carbon, <100% relative capacity	−1 to 0	(A) ionic Li^{+1}
	4 to <22	(B) inserted Li^{0-1}
amorphous deintercalated carbon	−1 to 0 (narrow)	(A) ionic Li, surface Li salts
	−1 to +1 (broad)	(A′) ionic Li, interface layer Li
dipped carbon electrode	−1 to 0 (narrow)	(A) ionic Li, surface Li salts

widths of species C and D, and (c) the respective contributions of species B−D to the total signal area as a function of temperature. From these results, several significant observations can be made. First of all, the line widths of both peaks D and C decrease dramatically within the temperature range 220 K $\leq T \leq$ 290 K. Second, as the temperature is increased, the frequency shift of peak C is accompanied by a redistribution in relative signal intensities such that this peak grows in intensity at the expense of peak B. This latter finding suggests the presence of some temperature-dependent exchange dynamics involving site C and at least part of species B, as discussed further below.

Figures 10 and 11 summarize analogous temperature-dependent studies on a 100% charged sample under static and MAS conditions, respectively. Note that similar temperature-dependent effects are observed here. In contrast to the situation in the 200% sample, the chemical shift of site **C** seems to reach a plateau value of ∼200 ppm at low temperatures. Also, sites A and B are better resolved under MAS conditions (Figure 11), and the reduction in relative intensity of site B is also evident at higher temperatures.

Discussion

Lithium Inventory in Li-Inserted Amorphous Carbons. The experimental results portray the following stages during the charging/discharging process: as an electrode is cycled between intercalated and deintercalated states, parasitic processes (corrosive hydration or oxidation effects) produce ionic lithium that is deposited on the surface in an oxide environment associated with the SEI layer (type A signal, see Figure 5). Lithium sites of type B are produced as the electrode is charged to levels less than 100% of maximum capacity. At or near 100% of relative charge, lithium of type C becomes evident. At charging capacities in excess of 100%, lithium metal begins to plate onto the electrode, and peak D is observed. The inventory of possible sites for lithium in the electrode materials and the corresponding ^{7}Li chemical shift ranges are summarized in Table 2.

On the basis of their NMR spectroscopic parameters, we assign lithium of type B to species intercalated between the graphene sheets, as their bonding properties appear to be similar to those present in lithium-graphite intercalation compounds

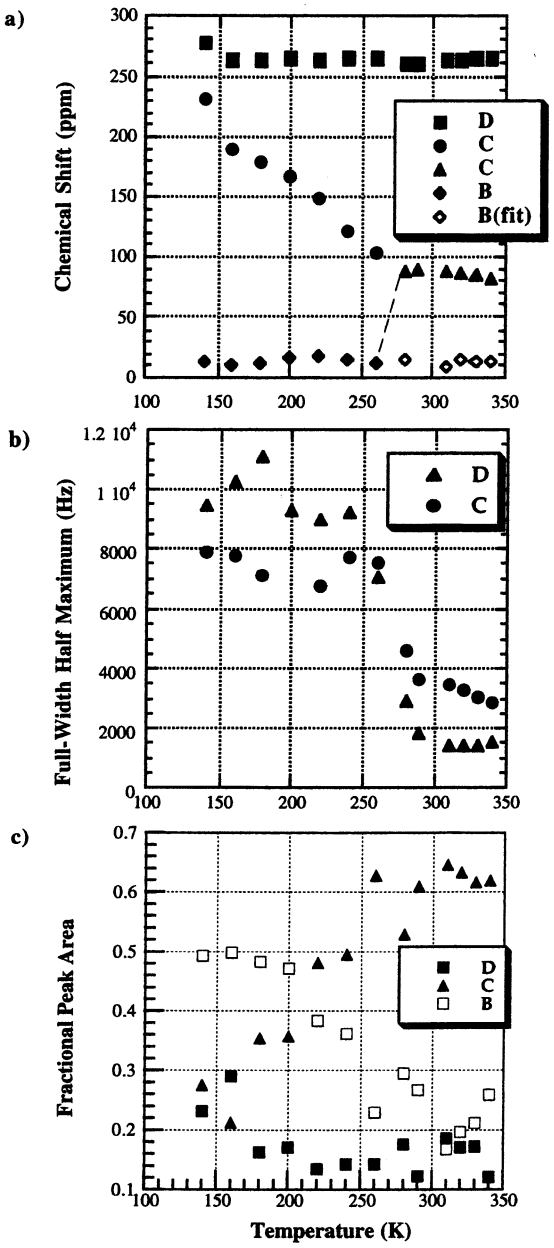

Figure 9. 200% charged carbon: (a) Temperature-dependent chemical shifts. For species C, the onset of exchange averaging is depicted by a change in symbol. (b) Peak width vs temperature for sites C (high-frequency inserted lithium) and D (metallic lithium). (c) Peak area vs temperature for sites B, C, and D.

(however, with smaller Knight shifts). At loading levels below that corresponding to 100% charging capacity, the chemical shift of this species is moderately dependent on lithium content, suggesting only subtle modifications of the lithium bonding state as a function of composition. The linear correlation observed in Figure 4c can be explained in terms of the Knight shift, which serves as a measure of s-electron density at the lithium nucleus. As the electrode material becomes more highly charged, more lithium has been inserted, and the increased chemical shift indicates a gradual increase of conduction electron density at the sites of the lithium nuclei. The effect may also reflect a reduction in average Li−Li distance. The monotonic dependence is in contrast to that in lithiated graphite where NMR chemical shifts have been observed for staged materials with discrete chemical shifts and a nonlinear trend with degree of intercalation. In lithiated graphite systems, "full" intercalation results in a stoichiometry of LiC_6, with a capacity of 372 mAh/g and

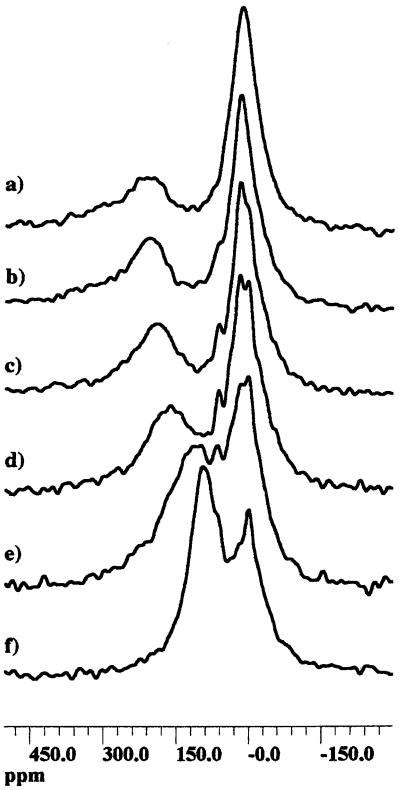

Figure 10. Variable temperature ^{7}Li static NMR spectra, 100% charged carbon electrode. (a) 140, (b) 170, (c) 200, (d) 230, (e) 260, and (f) 290 K.

a ^{7}Li NMR chemical shift of 44 ppm,[47] whereas higher stage compounds (e.g., LiC_{18}) give rise to resonances that are significantly smaller (such as 12−16 ppm).[48] The lower chemical shifts observed in the present materials may arise from lithium species sandwiched between graphene sheets in the carbon that are not as crystallographically ordered as those in graphite.

The appearance and the spectroscopic characteristics of peak C suggest the formation of dense lithium regions with lower carbon:lithium ratios than in LiC_6 that are semimetallic in character. The species formed in such lithium-rich regions are characterized by strong Li−Li electronic interactions, giving rise to NMR observables more similar to lithium metal than to lithium in graphite intercalation compounds.

This interpretation is suggested both by the high-frequency shifts and by the temperature-dependent reduction in line width. Site C exhibits a temperature-dependent Knight shift, and the magnitude of the shift at low temperatures is comparable to that of metallic lithium. This behavior reflects that the spin density localized on the lithium varies with temperature, thereby affecting the chemical shift. Similar temperature-dependent behavior has been documented for semimetallic lithium species in intercalation compounds, such as Chevrel phases of $Li_3Mo_6Se_8$[49,50] and Li_2VSe_2.[51] Such a large temperature-dependent shift would also be consistent with Curie paramagnetism, and coupling to a paramagnetic site cannot be fully ruled out without cooling the sample even further (the experimental apparatus permitted experiments only as low as 140 K). It is notable, however, that this temperature-dependent species is only observed in samples that have been charged to >100% of capacity, the point at which there is a high enough potential to produce metallic species at the anode. If paramagnetic interactions should occur, these would be expected with other sites (A−D), as well; yet, only site C exhibits this particular behavior.

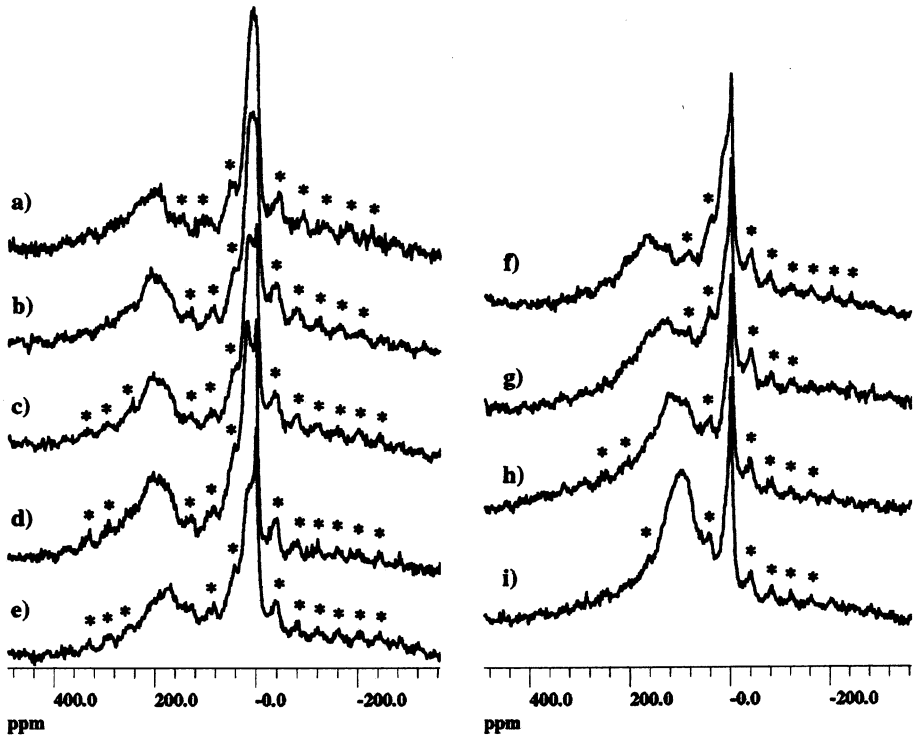

Figure 11. Variable temperature ^{7}Li MAS NMR spectra, 100% charged carbon electrode ($\nu_r = 4.8-5.1$ kHz). These spectra show the 9 ppm feature, B, and the high-frequency feature, C, more clearly. (a) 140, (b) 160, (c) 180, (d) 200, (e) 220, (f) 230, (g) 250, (h) 270, and (i) 290 K.

Furthermore, a temperature-dependent reduction in line width is observed for site C, depicted in Figure 9b. The effect observed here is attributed to motional narrowing owing to lithium diffusion, resulting in an averaging of the ^{7}Li−^{7}Li dipole−dipole interaction. Narrowing occurs for lithium metal (species D) and lithium species C in the same temperature range, showing that the diffusion processes in both types of lithium environments are characterized by similar activation energies. The similarity in the extent and the onset temperature of the line narrowing supports the idea that the interatomic interactions for the lithium atoms giving rise to peak C are similar in character to that in metallic lithium.

Altogether, these results suggest that site C may reflect small clusters of semimetallic Li formed in the microvoids of the amorphous carbon. It has been suggested that similar high-frequency resonances may arise from lithium dendrites.[52] However, the large line widths observed in our materials more likely reflect a heterogeneous size distribution of these lithium-filled microvoids and differences in local environments and electronic properties. Possibly, the bonding state evidenced for the type C lithium species can be compared to that of Li colloids, formed from irradiated Li_2O materials.[53,54]

The presence of such Li clusters could be further established through application of dipolar methods, such as ^{7}Li−^{6}Li SEDOR NMR, which is sensitive to Li−Li dipolar interactions and, consequently, interatomic distance distributions. We attempted such an experiment but found that the spin−lattice relaxation rates were too short for an effective SEDOR study. Work at lower temperatures could help resolve this issue.

The formation of lithium-rich clusters in amorphous Li−carbon materials has been proposed in other studies. Such proposals have included lithium micro- or nanoclusters in microcavities,[14,55] and flat Li_7 clusters with strong covalent bonding.[56] Such clusters can account for reversible intercalation to levels greater than LiC_6.[57,58] For example, Li intercalation into graphite under high-pressure resulted in phases described as LiC_2 and LiC_3 for which XPS spectra revealed low binding energies, reflecting a significant drop in the extent of charge transfer from Li to the carbon host.[59] This observation is very consistent with the high chemical shifts observed in our NMR study and other works. Finally, the low amount of charge transfer is clearly reflected in the charge/voltage curves, revealing a very low cycling potential at loading levels exceeding 100% reversible charge. Thus, all of these results support the formation of Li clusters in amorphous carbons charged to ≥100% relative capacity.

Although the results in this study are comparable to those obtained recently in other laboratories, the wide range of ^{7}Li chemical shifts realized with the present class of amorphous carbons is striking. Evidence of many of the observations presented by other groups can also be seen in the spectra for these carbons, indicative of the variety of chemical environments that are possible in the PMAN/DVB disordered carbons.

Dynamic Phenomena. Variable temperature NMR experiments over the range 140−400 K have served to illustrate particular behavior of the reversible lithium species in the two sites, B and C, as well as to probe irreversible chemical changes that occur with heating. Table 3 summarizes the temperature-dependent behavior of the various lithium species. The variable temperature data provide compelling evidence for the existence of dynamic exchange between sites B and C in these materials. At room temperature, the dominant contribution to the ^{7}Li signal arises from a dynamic exchange process involving site B and a high frequency site that is most clearly seen in the low temperature (below 200 K) spectra of the 100% charged carbon (see Figures 10 and 11). This process is also operative in the 200% charged carbon, although the low-temperature limit for peak C is not reached in the temperature range investigated (down to 140 K). Nevertheless, the trends observed in Figure 9, parts a and c, also support the concept of exchange in this sample. In both samples, a portion of peak B persists throughout the temperature range investigated, suggesting that some of the

TABLE 3: Temperature Dependent Effects on Lithium Species

site/temperature	^{7}Li chemical shift (ppm)	static line width
A (ionic lithium)	(temperature invariant)	
200−400 K	∼ −1 ppm	∼650 Hz
B (inserted lithium)	(temperature invariant)	
140−240 K	∼14 ppm	∼4600 Hz
C (within cluster)		
140−260 K	230−110 ppm	∼7700 Hz
280−330 K	∼92 ppm	4500−2850 Hz
340−400 K	85−14 ppm	not measured
D (metallic lithium)	(temperature invariant)	
140−240 K	∼262 ppm	∼10 500 Hz
240−310 K	∼262 ppm	9500−1400 Hz
310−340 K	∼262 ppm	∼1450 Hz
LiC_6	(temperature invariant)	
140−260 K	∼46 ppm	∼4300 Hz
260−300 K	∼46 ppm	4000−1900 Hz

B sites do not participate in the exchange process. We propose that these are attributable to inserted Li ions that are spatially remote from the Li clusters.

The idea of dynamic exchange between distinct lithium sites in amorphous carbons has already been proposed in several recent publications. The most clear evidence for this hypothesis was provided by Tatsumi et al.[44] on nongraphitizable (hard) carbons, pyrolyzed to 1200 °C and charged to a reversible capacity of $Li_{1.25}C_6$. In this case, straightforward line shape coalescence phenomena were observed, involving the entire Li population within the sample. A subsequent paper by these authors reported similar results (based on peak area analysis) in two different high-temperature pyrolyzed carbons (1000 and 1200 °C, fully lithiated).[57] A considerably more complex situation was reported by Guérin et al. (ref 45). These workers evaluated nongraphitizable (hard) carbons pyrolyzed at a range of temperatures and made assignments through deconvolutions of broad resonance lines. In contrast to our materials, their carbons incorporated various binders that were shown to have a substantial influence on the spectroscopic behavior observed. These samples showed multiple lithium environments, some of which are characterized by temperature-dependent chemical shifts, thereby complicating the analysis of the exchange phenomena. The situation present in the samples studied here is of comparable complexity, as we observe a combination of temperature-variant and invariant species.

Furthermore, the exchange effect observed in our samples depends on the lithium loading level. For 100% charged carbons, our results are comparable to those of Tatsumi et al., whereas for 200% charged carbons, the low-temperature limit of the exchange process has not been reached.

Finally, our results indicate that the inventory of reversible lithium sites is changing with time, and therefore, a chemically reacting system is being observed. By heating the sample during the course of a variable temperature experiment, this process can be accelerated, resulting in the irreversible disappearance of the Li clusters (and Li metal) and a concomitant increase in the population of site B, the inserted lithium species. Data from Figure 7d indicate that by putting a charged sample into contact with a deintercalated sample one stimulates the diffusion of lithium into unoccupied sites (site B).

Conclusions

Our results suggest that, beyond its utility for quantitatively discriminating between reversibly and irreversibly intercalated lithium species, ^{7}Li NMR is a very useful tool for assessing and differentiating between various types of inserted lithium species into amorphous carbon materials.

Lithium species that are irreversibly removed from the electrochemical intercalation cycle by parasitic processes can be identified and quantified. Furthermore, two types of reversible lithium species can be differentiated. At reversible capacities <100%, lithium ions populate sites with similar electronic and bonding characteristics as present in graphite intercalation compounds, whereas at higher reversible capacities, lithium-rich clusters are formed in addition. The high reversible capacities previously reported for Li-amorphous carbon insertion compounds are most likely due to the formation of such Li clusters.

Both of the inserted species are involved in dynamic exchange phenomena, which also facilitate a spatial redistribution of lithium over time. This results in long-term changes of the lithium bonding state and is likely to affect the electrochemical performance characteristics of highly loaded samples. The results of the present study indicate that, although the clusters belong to the inventory of reversible species on the time scale of electrochemical cycling experiments, these species are probably not long-lived enough to be relevant for battery applications.

Acknowledgment. The authors thank Anthony K. Cheetham for providing NMR facilities and lab space, at University of California Santa Barbara, Zhengming John Zhang for initial samples and helpful discussions, and Marion C. Hunter for sample synthesis and characterization. We also thank Herb Case and Michael Overstreet, Sandia National Laboratories, Albuquerque, who assisted with the testing of the Tee cells. Funding was provided by Sandia National Laboratories. Sandia National Laboratories is a multi-program laboratory operated by Sandia Corp., a Lockheed Martin company, for the United States Department of Energy under Contract DE-AC04-94AL85000. This work was partially supported by the MRL Program of the National Science Foundation under Award No. DMR96-32716.

References and Notes

(1) Yazami, R.; Touzain, P. *J. Power Sources* **1983**, *9*, 365−371.

(2) Billaud, D.; Henry, F. X.; Willmann, P. *Mol. Cryst. Liq. Cryst.* **1994**, *244*, A159−A164.

(3) Billaud, D.; Henry, F. X.; Willmann, P. *J. Power Sources* **1995**, *54*, 383−388.

(4) Besenhard, J. O. *Progress in Intercalation Research*; Müller-Warmuth, W., Schöllhorn, R., Eds.; Kluwer Academic Publisher: Dordrecht, The Netherlands, 1994; pp 457−508.

(5) Coa, F.; Barsukov, I. V.; Bang, H. J.; Zaleski, P.; Prakesh, J. *J. Electrochem. Soc.* **2000**, *14*, 3579.

(6) Guerard, D.; Lagrange, P.; El Makrini, M.; Herold, A. *Synth. Met.* **1981**, *3*, 15−19.

(7) Fischer, J. E. *Mater. Sci. Eng.* **1977**, *31*, 211−223.

(8) Pfluger, P.; Oelhafen, P.; Künzi, H. U.; Jeker, R.; Hauser, E.; Ackermann, K. P.; Müller, M.; Güntherodt, H.-J. *Physica B&C* **1980**, *99*, 395−400.

(9) Delhaes, P. *Mater. Sci. Eng.* **1977**, *31*, 225−234.

(10) Delhaes, P.; Manceau, J. P.; Guerard, D. *Synth. Met.* **1980**, *2*, 277−284.

(11) Charlier, A.; Charlier, M. F.; Fristot, D. *J. Phys. Chem. Solids* **1989**, *50*, 987−996.

(12) Dahn, J. R.; Reimers, J. N.; Tiedje, T.; Gao, Y.; Sleigh, A. K.; McKinnon, W. R.; Cramm, S. *Phys. Rev. Lett.* **1992**, *68*, 835−838.

(13) Boersma, M. A. M. *Catal. Rev.−Sci. Eng.* **1974**, 243−256.

(14) Takami, N.; Satoh, A.; Ohsaki, T.; Kanda, M. *Electrochim. Acta* **1997**, *42*, 2537−2543.

(15) Yata, S.; Hato, Y.; Kinoshita, H.; Ando, N.; Anekawa, A.; Hashimoto, T.; Yamaguchi, M.; Tanaka, K.; Yamabe, T. *Synth. Met.* **1995**, *73*, 273−277.

(16) Zheng, T.; Reimers, J. N.; Dahn, J. R. *Phys. Rev. B* **1995**, *51*, 734−741.

(17) Yazami, R.; Cherigui, A.; Nalimova, V. A.; Guerard, D. In *Proc. Symp. on Lithium Batteries*; Surampudi, S., Koch, V. R., Eds.; The Electrochemical Society: Pennington, NJ, 1993; pp 1−8.

(18) Imoto, H.; Omaru, A.; Azuma, H.; Nishi, Y. In *Proc. Symp. on Lithium Batteries*; Surampudi, S., Koch, V. R., Eds.; The Electrochemical Society: Pennington, NJ, 1993; pp 9−31.
(19) Huang, C. K.; Surampudi, S.; Attia, A.; Halpert, G. In *Proc. Symp. on Lithium Batteries*; Surampudi, S., Koch, V. R., Eds.; The Electrochemical Society: Pennington, NJ, 1993; pp 32−43.
(20) Takami, N.; Sato, A.; Ohsaki, T. In *Proc. Symp. on Lithium Batteries*; Surampudi, S., Koch, V. R., Eds.; The Electrochemical Society: Pennington, NJ, 1993; p 44.
(21) Dahn, J. R.; Sleigh, A. K.; Shi, H.; Reimers, J. N.; Zhong, Q.; Way, B. M. *Electrochim. Acta* **1993**, *38*, 1179−1191.
(22) Even, W. R.; Gregory, D. P. *MRS Bull.* **1994**, *19*, 29−33.
(23) Dai, Y.; Wang, Y.; Eshkenazi, V.; Peled, E.; Greenbaum, S. G. *J. Electrochem. Soc.* **1998**, *145*, 1179−1183.
(24) Newnham, C. E.; Rinne, S.; Scholey, N. *J. Power Sources* **1995**, *54*, 516−518.
(25) Iijima, T.; Suzuki, K.; Matsuda, Y. *Synth. Met.* **1995**, *73*, 9−20.
(26) Alcántara, R.; Fernández Madrigal, F. J.; Lavela, P.; Tirado, J. L.; Jiménez Mateos, J. M.; Gómez de Salazar, C.; Stoyanova, R.; Zhecheva, E. *Carbon* **2000**, *38*, 1031−1041.
(27) Tatsumi, K.; Kawashita, N.; Sakaebe, H.; Shioyama, H.; Higuchi, S.; Mabuchi, A.; Fujimoto, H. *J. Electrochem. Soc.* **1995**, *142*, 716−720.
(28) Tatsumi, K.; Akai, T.; Imamura, T.; Zaghib, K.; Iwashita, N.; Higuchi, S.; Sawada, Y. *J. Electrochem. Soc.* **1996**, *143*, 1923−1930.
(29) Kuribayashi, I.; Yokoyama, M.; Yamashita, M. *J. Power Sources* **1995**, *54*, 1−5.
(30) Yamamoto, O.; Imanishi, N.; Takeda, Y.; Kashiwagi, H. *J. Power Sources* **1995**, *54*, 72−75.
(31) Hayes, S.; van Wüllen, L.; Eckert, H.; Even, W. R.; Crocker, R. W.; Zhang, Z. *Chem. Mater.* **1997**, *9*, 901−911.
(32) Sato, K.; Noguchi, M.; Demachi, A.; Oki, N.; Endo, M. *Science* **1994**, *264*, 556−558.
(33) Eckert, H. *Prog. NMR Spectrosc.* **1992**, *24*, 159−293.
(34) Pietrass, T.; Taulelle, F.; Lavela, P.; Olivier-Fourcade, J.; Jumas, J.-C.; Steuernagel, S. *J. Phys. Chem. B* **1997**, *101*, 6715−6723.
(35) Prigge, C.; Müller-Warmuth, W.; Schöllhorn, R. *Z. Phys. Chem.* **1995**, *189*, 153−168.
(36) Carver, G. P. *Phys. Rev. B* **1970**, *2*, 2284−2295. Müller-Warmuth, W. In *Progress in Intercalation Research*, Müller-Warmuth, W., Schöllhorn, R., Eds.; Kluwer Academic Publishers: Norwell, MA, 1994; pp 339−455.
(37) Mori, Y.; Iriyama, T.; Hashimoto, T.; Yamazaki, S.; Kawakami, F.; Shiroki, H.; Yamabe, T. *J. Power Sources* **1995**, *56*, 205−208.
(38) Tatsumi, K.; Kawamura, T.; Higuchi, S.; Hosotubo, T.; Nakajima, H.; Sawada, Y. *J. Power Sources* **1997**, *68*, 263−266.
(39) Nakagawa, Y.; Wang, S.; Matsumura, Y.; Yamaguchi, C. *Synth. Met.* **1997**, *85*, 1363−1364.
(40) Yoshio, M.; Wang, H.; Fukuda, K.; Hara, Y.; Adachi, Y. *J. Electrochem. Soc.* **2000**, *145*, 1245−1250.
(41) Zaghib, K.; Tatsumi, K.; Sawada, Y.; Higuchi, S.; Abe, H.; Ohsaki, T. *J. Electrochem. Soc.* **1999**, *146*, 2784−2793.
(42) Tatsumi, K.; Akai, T.; Higuchi, S.; Sawada, Y.; Kawamura, T.; Hosotubo, T.; Nakajima, H. *Extended Abstr. 8th Int. Meeting Lithium Batteries* **1996**, 210−211.
(43) Takami, N.; Satoh, A.; Oguchi, M.; Sasaki, H.; Ohsaki, T. *J. Power Sources* **1997**, *68*, 283−286.
(44) Tatsumi, K.; Conard, J.; Nakahara, M.; Menu, S.; Lauginie, P.; Sawada, Y.; Ogumi, Z. *Chem. Commun.* **1997**, 687−688.
(45) Guérin, K.; Ménétrier, M.; Février-Bouvier, A.; Flandrois, S.; Simon, B.; Biensan, P. *Solid State Ionics* **2000**, *127*, 187−198.
(46) Yamazaki, S.; Hashimoto, T.; Iriyama, T.; Mori, Y.; Shiroki, H.; Tamura, N. *J. Mol. Struct.* **1998**, *441*, 165−171.
(47) Lauginie, P.; Letellier, M.; Estrade, H.; Conard, J.; Guerard, D. *Proc. 5th Int. Carbon Graphite Conf. Vol. II* **1978**, 645−653.
(48) Conard, J.; Estrade, H. *Mater. Sci. Eng.* **1977**, *31*, 173−176.
(49) Aselmann, G.; Müller-Warmuth, W. *Z Phys Chem Neue Fol* **1987**, *151*, 103−111.
(50) Prigge, C.; Müller-Warmuth, W.; Gocke, E.; Schollhorn, R. *Chem. Mater* **1993**, *5*, 1493−1498.
(51) Prigge, C.; Müller-Warmuth, W. *Z. Phys Chem* **1995**, *189*, 153−168.
(52) Gerald, R. E.; Klingler, R. J.; Sandí, G.; Johnson, C. S.; Scanlon, L. G.; Rathke, J. W. *J. Power Sources* **2000**, *89*, 237−243.
(53) Beuneu, F.; Vajda, P.; Zogol, O. P. *Colloid Surf. A* **1999**, *158*, 83−87.
(54) Beuneu, F.; Vajda, P. *Phys. Rev. Lett.* **1996**, *76*, 4544−4547.
(55) Mabuchi, A.; Tokumitsu, K.; Fujimoto, H.; Kasuh, T. *J. Electrochem. Soc.* **1995**, *142*, 1041−1046.
(56) Setton, R.; Conard, J. *Mol. Cryst. Liq. Cryst. A* **1994**, *244*, 307−312.
(57) Yazami, R.; Deschamps, M. *Rechargeable Lithium and Lithium-Ion Batteries*; Megahed, S., Barnett, B. M., Xie, L., Eds.; The Electrochemical Society Proceedings Series: Pennington, NJ, 1994; PV 94−28, pp 183−XXX.
(58) Yata, S.; Kinoshita, H.; Komori, M.; Ando, N.; Yamabe, T. *Synth. Met.* **1994**, *62*, 153−158.
(59) Mordkovich, V. Z. *Synth. Met.* **1996**, *80*, 243−247.
(60) Tatsumi, K.; Conard, J.; Nakahara, M.; Menu, S.; Lauginie, P.; Sawada, Y.; Ogumi, Z. *J. Power Sources* **1999**, *82*, 397−400.